J Appl Physiol 105: 1881–1888, 2008.
First published October 9, 2008; doi:10.1152/japplphysiol.90792.2008.

Altered collagen fiber kinematics define the onset of localized ligament damage during loading

Kyle P. Quinn and Beth A. Winkelstein

Spine Pain Research Laboratory, Departments of Bioengineering and Neurosurgery, University of Pennsylvania, Philadelphia, Pennsylvania

Submitted 19 June 2008; accepted in final form 2 October 2008

Quinn KP, Winkelstein BA. Altered collagen fiber kinematics define the onset of localized ligament damage during loading. *J Appl Physiol* 105: 1881–1888, 2008. First published October 9, 2008; doi:10.1152/japplphysiol.90792.2008.—Detecting the initiation of mechanical injury to biological tissue, and not just its ultimate failure, is critical to a sensitive and specific characterization of tissue tolerance, development of quantitative relationships between macro- and microstructural tissue responses, and appropriate interpretation of physiological responses to loading. We have developed a novel methodological approach to detect the onset and spatial location of structural damage in collagenous soft tissue, before its visible rupture, via identification of atypical regional collagen fiber kinematics during loading. Our methods utilize high-speed quantitative polarized light imaging to identify the onset of tissue damage in ligament regions where mean collagen fiber rotation significantly deviates from its behavior during noninjurious loading. This technique was validated by its ability to predict the location of visible rupture ($P = 0.0009$). This fiber rotation-based metric of damage identifies potential facet capsular ligament injury beginning well before rupture, at $51 \pm 12\%$ of the displacement required to produce tissue failure. Although traditional macroscale strain metrics fail to identify the location of microstructural damage, initial injury detection determined by altered fiber rotation was significantly correlated ($R = 0.757$, $P = 0.049$) with tissue yield (defined by a decrease in stiffness), supporting the capabilities of this method. Damaged regions exhibited higher variance in fiber direction than undamaged regions ($P = 0.0412$).

mechanics; strain; mechanical trauma; quantitative polarized light imaging

TISSUE INJURY RESULTING FROM mechanical trauma has traditionally been defined by gross measures of mechanical failure and/or evidence of a visible rupture of a tissue (21, 40). However, these conventional indicators of mechanical injury may not actually identify the tissue's tolerance to injury. Subfailure loads can produce a variety of altered mechanical phenomena in ligaments and tendons, including increased laxity (20, 30, 33, 35), decreased stiffness (29, 35, 36), and altered viscoelastic responses (29). These mechanical responses are also coupled with the onset of pathophysiological conditions, such as collagen disorganization (15, 36), fibroblast necrosis (35), and nociceptor activation (25). Although these studies collectively identify a host of mechanical and physiological changes in soft tissue for certain subfailure loading cases, they cannot directly identify the initiation of local microstructural damage in the tissue. This inability to directly detect or localize injury could result in the mischaracterization of injury thresholds and/or focus efforts for prevention or treatment of tissue pathology in the wrong tissue regions.

Because it is not possible to visualize and identify subfailure damage as it occurs, macroscale strain metrics, such as maximum principal strain, are commonly used to establish injury criteria and tolerances and to identify the location of potential tissue injury (1, 14, 24, 25, 40, 51). However, macroscopic strain fields in ligaments and tendons may lack the sensitivity to localize microstructural damage or, in some cases, gross rupture due to collagen fiber movement or high spatial variability in the strain field (8, 32, 36, 39). Therefore, detecting the initiation of soft tissue damage during mechanical loading, rather than estimating strains or the resultant structural effects of injurious loading, is critical to the sensitive and specific characterization of tissue injury tolerance and development of truly integrative mechanistic relationships between tissue loading, micromechanics, physiological responses, and the interactions between each of these.

A variety of noninvasive imaging techniques have been utilized to quantify tissue microstructure or fiber alignment, including optical coherence tomography, electron microscopy, X-ray diffraction, diffusion tensor magnetic resonance imaging, and nonlinear optical microscopy (17–19, 27, 38, 48, 50, 52). Although these techniques allow for the acquisition and quantification of a variety of microstructural components at different loading conditions, few of them can facilitate a continuous assessment of fiber alignment during loading. Polarized light has been used to determine fiber organization, kinematics, and crimp patterns in soft tissues, such as tendons, ligaments, and heart valves, by taking advantage of collagen's birefringence (10, 42–45, 49). Tower et al. (43) developed a quantitative polarized light imaging (QPLI) system capable of determining collagen fiber alignment maps in soft tissue during continuous loading. Although Tower et al. demonstrated complex fiber realignment during tissue loading up to its rupture, no study has used QPLI or any other optical technique to specifically detect and/or quantify the initial occurrence of localized damage during ligament loading.

QPLI provides the ideal approach to identify microstructural damage by evaluation of entire regions of the ligament surface area during loading via the acquisition of continuous fiber information with pixel-level resolution. This technique is ideally suited for determination of the preferred fiber direction in any relatively planar tissue through which light can be transmitted and for which linear birefringence dominates the optical response. Given that mechanical injury to the facet joint's

Address for reprint requests and other correspondence: B. A. Winkelstein, Dept. of Bioengineering, Univ. of Pennsylvania, 240 Skirkanich Hall, 210 S. 33rd St., Philadelphia, PA 19104-6321 (e-mail: winkelst@seas.upenn.edu).

The costs of publication of this article were defrayed in part by the payment of page charges. The article must therefore be hereby marked "*advertisement*" in accordance with 18 U.S.C. Section 1734 solely to indicate this fact.

capsular ligament has been proposed to occur during some subfailure loading scenarios (6, 23, 25, 31, 51, 53), this ligament serves as an ideal tissue for localizing subfailure microstructural tissue damage via a QPLI approach. Despite many anatomic, histological, and biomechanical studies characterizing the cervical facet capsule (6, 9, 25, 31, 36, 40, 51, 53), there are no reports detailing the fiber orientation of the human facet capsular ligament. Capsuloligamentous material, because of its functional demands, generally demonstrates greater spatial variability in fiber direction than more organized cablelike ligaments; the planar geometry of the human facet capsule makes it more amenable than other more organized ligaments to the QPLI experimental technique. Our overall hypothesis is that damage to facet capsule tissue can be detected before visible gross rupture of the ligament by quantification of the regional fiber kinematics of the collagen matrix during loading. As such, the primary goal of this study was to utilize QPLI to develop optical injury detection methods and metrics capable of identifying structural damage in the human facet capsular ligament. Specifically, fiber alignment was quantified and summarized in different regions covering the lateral face of the ligament during tensile loading. Damage was identified by significant increases in the rotation of the regional mean fiber directions, and validation of this method of damage detection was also performed through a direct comparison with the location of visible tissue rupture. The loading conditions and location at which damage was first detected were also compared with conventional mechanical measures of injury, including tissue yield and macroscale strain fields. Application of this fiber rotation-based metric to detect damage enables a detailed and specific characterization of a class of mechanical injuries that have not been previously identified, largely because existing methods lack the sensitivity and specificity to detect the occurrence of microstructural failure.

METHODS

Specimen preparation and integrated QPLI mechanical testing system. Isolated right and left facet joints ($n = 8$) were removed en bloc from the C_4/C_5 spinal motion segments of five fresh, unembalmed human cadavers (59 ± 12.8 yr of age; obtained from the International Institute for the Advancement of Medicine). Through fine dissection, all musculature and tendon insertions on the surface of the facet capsules were removed. The posterior side of the lateral aspect of the facet capsule was isolated for testing, and all other regions of the capsule were transected. Portions of the superior and inferior articular processes of the joint were removed to facilitate the transmission of polarized light through the ligament tissue. In addition, an array of 15–24 fiduciary markers was applied to the ligament using a 0.2-mm-diameter felt-tip pen to track tissue deformation and estimate strain fields during loading (Fig. 1). Dental stone was used to cast the bony ends of the specimens in testing cups, which were mounted to a testing machine (model 5385, Instron, Norwood, MA).

Before mechanical testing, sample width and thickness were measured with digital calipers, and the average cross-sectional area was calculated assuming a rectangular shape for the unloaded tissue. To provide a consistent initial position for all samples, we applied a 5-kPa preload to establish a reference condition and to define the initial joint displacement for each specimen. Specimens were preconditioned with 30 cycles of tensile loading between 0 and 0.5 mm (producing loads <5% of the failure load for this ligament). After preconditioning, specimens were distracted in tension at 0.5 mm/s until gross failure of the ligament was produced. Load and displacement data were collected at 1 kHz.

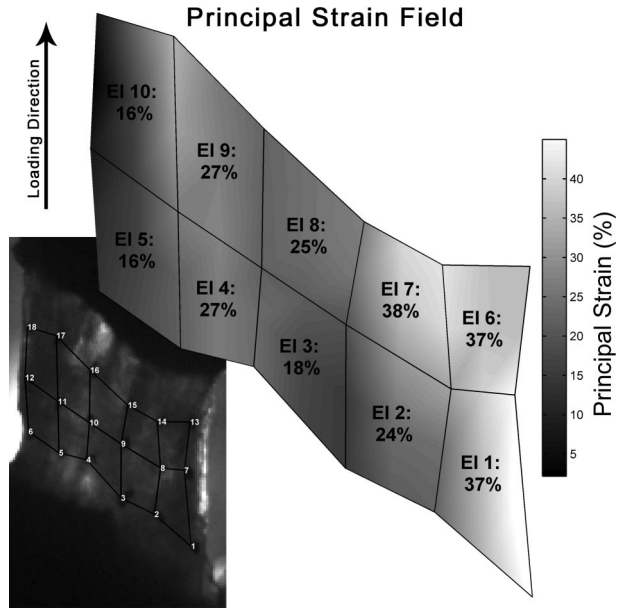

Fig. 1. Image of a typical specimen (*C390-C45L*) showing region definitions and corresponding principal strain field at initial detection of damage. On the basis of displacement of fiduciary markers (*bottom left*), principal strain was computed following construction of 4-node elements. Principal strain of each element is indicated on the strain field and expressed as a percentage. Maximum principal strain at initial detection of damage was 38% for this specimen and is located in *element 7* (El 7).

A QPLI system, enabling the simultaneous acquisition of mechanical, fiber alignment, and strain data, was assembled based on the design reported by Glazer et al. (16) and Tower et al. (43). It was modified to operate and interface with the Instron testing machine. For our system, a stepper motor-driver-controller system (NEMA 17, Lin Engineering, Santa Clara, CA) rotates a 20-cm cast acrylic disk equipped with a linear polarizing laminated film (Edmund Optics, Barrington, NJ). A fiber-optic illuminator with focusing lens (Edmund Optics) provides a light source behind the rotating polarizer to transmit light through the ligament. A circular analyzer was constructed using a mica quarter-wave plate (Optosigma, Santa Ana, CA) and linear polarizing film to analyze the polarized light transmitted through the ligament. For this study, the circular analyzer was aligned and mounted to a ×6 macrozoom lens and a high-speed charge-coupled device (CCD) camera (Vision Research, Wayne, NJ).

A two-camera system (Phantom versions 5.1 and 4.3, Vision Research, Wayne, NJ) was used to collect polarized light data and was synchronized with the acquisition of mechanical data: one CCD camera imaged the ligament deformation and acquired polarized light data, and the other CCD camera monitored the position of the rotating polarizer. The CCD cameras collected images with a field of view of 1.75 × 3.60 cm and 11 pixel/mm resolution; light intensity was stored with 8-bit resolution. All images were acquired at 500 frames/s, while the linear polarizer rotated at 750 rpm. This setup produced a set of 20 images that were acquired every 40 ms as the polarizer rotated through 180°. Each set of 20 images was used to create a single map of fiber alignment corresponding to every 0.02 mm of distraction.

Mechanical data analysis. Gross failure of the ligament was defined to occur at the maximum force value recorded, and the corresponding displacement and energy to failure were measured at this point for each specimen. To provide the most conservative detection of a loss of microstructural integrity using the force-displacement data, the first occurrence of ligament yielding was defined based on a decrease in stiffness (37, 54). Tangent stiffness was calculated at each data point using a centered finite-difference approximation (37): $k_i = (F_{i+1} - F_{i-1})/(\delta_{i+1} - \delta_{i-1})$, where the stiffness ($k_i$) at a given

point i was calculated from the difference in force (F) and displacement (δ) between the previous ($i - 1$) and following ($i + 1$) data points. Ligament yield was defined as the point at which the tangent stiffness first began to decrease by $\geq$10% of its peak value during distraction (37). The force and displacement at yield and the energy to yield were also recorded for comparison with the collagen fiber data.

Planar tissue deformation during distraction was quantified using the fiduciary markers on the capsule surface in the QPLI images. Marker locations were digitized and tracked during tissue loading, and the capsule surface was divided into regions by construction of four-node elements from the fiduciary marker locations (Fig. 1). Through isoparametric mapping, Lagrangian strain was computed for each element for every 0.02 mm of distraction. The element(s) with the maximum principal strain and maximum shear strain was noted in every image.

Collagen fiber analysis and damage detection. For analysis of the fiber alignment in the ligament tissue, harmonic analysis was employed to generate alignment maps (45) over the duration of the ligament distraction. The intensity (I) of each pixel in any set of consecutive images was described by the harmonic relationship

$$I(\theta_i) = A + B\cos(2\theta_i) + C\sin(2\theta_i) \quad (1)$$

where θ_i indicates the polarizer rotation angle with respect to horizontal at each interval i, A represents the mean intensity, and B and C are the signed harmonic amplitudes. The Fourier coefficients, A, B, and C, were determined using a summation approximation and scaled by pixel intensity (43, 45). Coefficients B and C were used to calculate the retardation (δ) of light, an indication of the strength of fiber alignment through the tissue thickness, and the fiber alignment direction (α) at each pixel using the following equations (13, 16, 43):

$$\delta = \cos^{-1}(\sqrt{1 - B^2 - C^2}) \quad (2)$$

$$\alpha = \frac{1}{2}\tan^{-1}(B/ - C) \quad (3)$$

With use of this approach, error measurement of the fiber alignment direction (α) is a function of the amplitude of light intensity. The mean error in measuring direction exceeds 9° when the peak-to-peak amplitude of a pixel is <6 (of 255) for our system; pixels determined to have amplitudes lower than that were not included in further fiber direction analysis.

Regional increases in the mean fiber rotation were used to identify the occurrence and location of structural damage in the ligament. Ligament regions for collagen fiber analysis were defined by the same four-node elements used in the strain analysis (Fig. 1). Within each of these elements, the mean fiber direction, variance in direction, and mean retardation were each computed on the basis of circular statistics for every 0.02-mm increment during the distraction of each specimen. The mean fiber directions were filtered using a 41st-order generalized Butterworth filter with a 2.5-Hz cutoff frequency and then differentiated with respect to displacement using the same centered finite-difference approach used for the mechanical data analysis to quantify the rotation of the mean fiber direction within each element during loading.

Structural damage was defined to occur in an element when the fiber rotation in that element exceeded its mean response by four standard deviations. For each element at a given displacement, the measurement of standard deviation was based on the distribution of all rotation data from the start of loading to that displacement. These region- and displacement-specific measures of standard deviation were calculated on the basis of the assumption that the mean fiber rotation was not biased toward clockwise or counterclockwise rotation and, so, had a normal distribution about a mean of zero. This assumption was validated through a z-test using rotation data from all elements and ensured that only an increase in the magnitude of rotation would be detected as damaged. Damage was defined to occur when the mean fiber rotation of any element first exceeded four standard deviations ($P < 0.0001$), which minimized the detection of false-positive values as the number of data points increases with increasing distraction. The displacement, force, and energy at the initial detection of damage were recorded, and each element of the ligament in which damage was detected was noted. The standard deviation measures for each region at the point of initial damage detection were used to detect additional damage during further loading up to and including gross failure.

Statistical analysis. The displacements at which initial damage, yield, and failure occurred were compared with each other using a one-way ANOVA and post hoc Bonferroni's corrections to determine whether each of these phenomena occur at different distractions. To validate the ability of our rotation-based damage metric to localize damage, we used Fisher's exact test to compare the elements identified as damaged at gross failure with the elements where rupture was first visible from the video data. To further determine the effectiveness of this damage metric, we estimated the strength of association between the detection of damage at failure and evidence of visible rupture by computing the odds ratio of successfully classifying an element as damaged or undamaged. At the displacement where initial damage was detected for each specimen, fiber alignment and strain measurements were compared between damaged and undamaged elements to evaluate other metrics as having the potential to identify damage. The absolute value of fiber rotation, variance in fiber direction, mean retardation, the offset of the mean fiber direction from specimen loading direction, principal strain, and maximum shear strain were compared. For each of these outcomes, significant differences between damaged and undamaged elements and between specimens were determined by an ANOVA with elements nested within specimens. Significance for each ANOVA was defined by $P < 0.05$; all tests were performed using JMP 7 (SAS Institute, Cary, NC).

RESULTS

The average width and thickness of the eight capsular ligament specimens were 7.46 ± 1.38 mm and 0.43 ± 0.92 mm, respectively, which correspond to a mean cross-sectional area of 3.2 ± 0.9 mm^2. At the reference displacement, an average of 11.0 ± 2.1 elements covered a surface area of 26.3 ± 12.1 mm^2 in each ligament midsubstance, and collagen fiber direction could accurately be detected by the QPLI system in an average of 89.5 ± 3.9% of the midsubstance area for all specimens. Gross structural failure of the ligament was detected at 21.62 ± 8.96 N and 3.67 ± 0.49 mm, and the energy required for failure was 28.99 ± 14.10 mJ (Table 1, Fig. 2). Ligament yield was first detected at 1.81 ± 0.65 mm of distraction and was significantly lower ($P < 0.001$) than the displacement at failure. The displacement at yield corresponded to a force of 8.31 ± 6.70 N and a mean energy to yield of 4.57 ± 4.22 mJ (Table 1). In four specimens, rupture was visible after failure within the elements covering the ligament midsubstance where collagen fiber alignment was being measured using the QPLI system. However, two specimens ruptured in the midsubstance just superior or inferior to the element regions being measured by QPLI, and one specimen ruptured near the ligament insertion to the C_5 bone. The ligament remained intact over the entire imposed loading for one specimen (*C457-C45L*), but structural failure occurred as a fracture in the C_5 articular bone. No ruptures were visible from the video data at yield for any specimen.

The use of increased fiber rotation as a metric of damage was validated on the basis of its ability to predict the location of visible tissue rupture after structural failure. For all four spec-

Table 1. *Summary of tissue mechanics at failure, yield, and initial detection of damage*

	Failure			Yield			Detected Damage		
Specimen No.	Force, N	Disp, mm	Energy, mJ	Force, N	Disp, mm	Energy, mJ	Force, N	Disp, mm	Energy, mJ
C390-C45L	25.43	4.13	34.87	13.84	2.92	9.93	9.03	2.51	5.33
C457-C45R	34.69	3.96	59.03	12.73	1.70	5.47	15.52	1.87	7.85
C846-C45L	27.04	3.23	26.62	19.54	2.61	11.51	11.15	2.18	4.95
C846-C45R	16.84	4.31	31.44	3.33	1.41	1.36	4.16	1.62	2.13
C947-C45R	11.60	3.59	15.93	1.49	1.18	0.57	4.96	2.12	3.39
C500-C45L	14.19	3.74	23.45	6.16	1.91	3.86	4.97	1.69	2.65
C500-C45R	12.37	3.55	13.57	0.44	1.10	0.15	0.67	1.30	0.26
*C457-C45L**	30.76	2.81	27.04	8.91	1.64	3.75	N/A	N/A	N/A
Mean	21.62	3.67	28.99	8.31	1.81	4.57	7.21	1.90	3.80
SD	8.96	0.49	14.10	6.70	0.65	4.22	5.00	0.41	2.48

Force, displacement (Disp), and energy were determined for each event. *Bone fractured at failure, no ligament rupture noted.

imens in which rupture occurred within an element being analyzed by QPLI, the fiber rotation-based metric also detected damage in that element at tissue failure (Fig. 3). Of the four other specimens in which rupture occurred outside the elements measured by the QPLI system, damage was detected only once in an element at failure. All the elements monitored from all specimens were considered, the damage detection data at failure were placed in a contingency table, and the detected location of damage at failure was significantly associated with the location of visible tissue rupture ($P = 0.0009$). The odds of an element being correctly identified by our damage metric as one where rupture would or would not occur were 25.7:1, suggesting a strong association between the two measures.

The rotation-based metric identified initial damage at a mean displacement of 1.90 ± 0.41 mm for seven of the eight specimens. No ligament damage was detected at any point during loading in one specimen (*C457-C45L*), which is consistent with no ligament rupture at failure for that specimen. Initial damage was detected significantly before gross failure ($P < 0.001$), but not before yield. The displacements at which damage and yield were detected were significantly correlated ($R = 0.757$, $P = 0.049$). The mean values for force at initial damage (7.21 ± 5.00 N) and energy required to produce damage (3.80 ± 2.48 mJ) were lower than those for yield.

The elements detected as damaged by significant mean fiber rotation also exhibited fiber alignment properties that were different from those of the undamaged elements. Damaged elements exhibited significantly larger ($P = 0.0025$) fiber rotation values than their undamaged counterparts (102.0 ± 66.3 vs. 29.4 ± 46.5°/mm; Table 2). These damaged elements also demonstrated a partial reorganization of fiber alignment (Fig. 4) that persisted during further loading of the tissue (*elements 3, 4*, and *9* in Fig. 5). For each specimen at the first detection of damage, the variance in fiber direction (Table 2) was significantly greater ($P = 0.0412$) in the damaged element than in the other elements that were deemed undamaged (mean variance = 0.827 ± 0.074 vs. 0.472 ± 0.238). Although the variance was higher in the damaged elements, the spatial distribution of fiber directions was not random but, rather, was due to the orientation of different fiber populations in nearly orthogonal directions (Figs. 4 and 5).

Although fiber alignment in the damaged and undamaged elements was different, retardation and the macroscale strain metrics were not different between these two groups of elements. Specifically, mean retardation between those elements initially identified as damaged (13.8 ± 4.2°) and those not

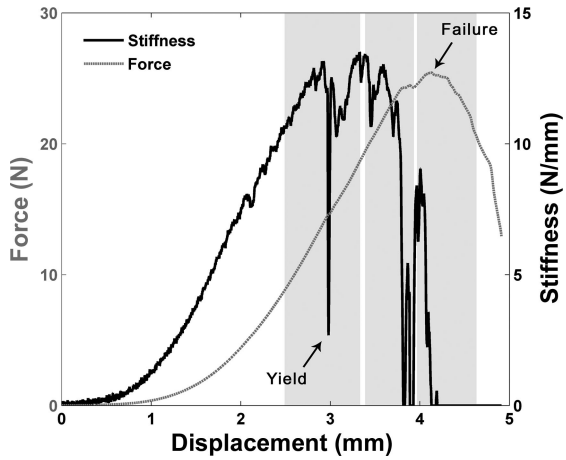

Fig. 2. Structural response of *specimen C390-C45L* during tensile distraction to failure. Maximum force value on force-displacement trace defines gross failure of the specimen. Stiffness-displacement curve is used to determine when yield occurs. Initial loss of stiffness at yield (2.92 mm) is ultimately recovered with increasing distraction. Shaded areas indicate displacements where damage was detected by fiber rotation.

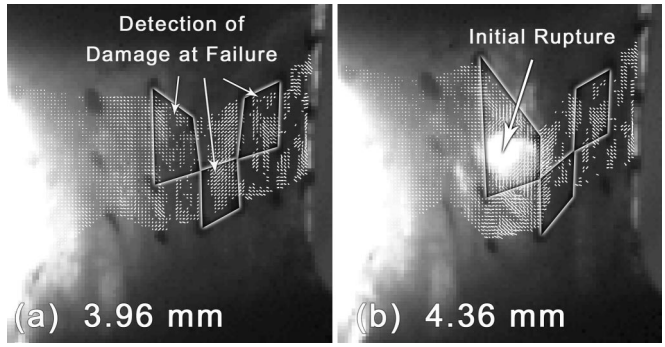

Fig. 3. Fiber alignment maps of *specimen C457-C45R* at failure (*a*) and 0.4 mm after failure (*b*). At the point of failure (3.96 mm, a), 3 elements were identified as damaged (arrows) on the basis of the rotation of their mean fiber direction. After additional ligament distraction (*b*), rupture was clearly visible as a large hole in one of those elements damaged at failure in *a*. Rupture was not visible in the 2 other elements identified in *a*, but development of the hole in *b* may have prevented the microstructural damage detected in these other elements in *a* from propagating into visible ruptures.

Table 2. *Summary of strain and fiber measurements from damaged and undamaged elements at initial detection of damage*

Outcome	Damaged Elements (n = 7)	Undamaged Elements (n = 73)
Fiber rotation,* °/mm	102.0±66.3	29.4±46.5
Variance in direction*	0.827±0.074	0.472±0.238
Offset of mean direction from specimen loading, °	42.9±34.5	43.1±25.1
Mean retardation, °	13.8±4.2	12.5±6.1
Principal strain, %	18.2±11.1	22.9±17.0
Maximum shear strain, %	14.0±6.1	15.8±7.8

Values are means ± SD. *Significantly different.

damaged (12.5 ± 6.1°) was not significantly different (Table 2). The mean values of principal strain (18.2 ± 11.1%) and maximum shear strain (14.0 ± 6.1%) in the damaged elements were not significantly different from those of the nondamaged elements (22.9 ± 17.0% and 15.8 ± 7.8%, respectively). Furthermore, the location of neither maximum principal strain nor maximum shear strain corresponded to elements with initial damage for any specimen (Figs. 1, 4, and 5). At failure, locations of maximum principal and shear strains matched locations of visible rupture in only two specimens.

DISCUSSION

This study uses QPLI techniques to localize damage in ligament tissue that has been otherwise undetectable and occurs during loading well below tissue failure (Fig. 1, Table 1). The initial detection of damage is significantly correlated (R = 0.757) with the occurrence of yield (defined by a decrease in stiffness), which supports the notion that this damage detection metric is sensitive to a loss of structural integrity, even at loading magnitudes well below failure or the onset of visible rupture of the tissue. The demonstration of significantly altered fiber kinematics near or before yielding of a ligament (Fig. 2, Table 1) also suggests that identifying the occurrence of yield may provide more appropriate estimates of structural tolerance than gross failure. Although there appears to be a relationship between regional fiber kinematics and damage, the element where initial damage was identified differed from the site of maximum principal strain (Figs. 1 and 4). Although the onset of damage was correlated with the macroscale mechanical response of yield, the discrepancy between strain and damage detection in this study suggests that traditional macroscale strain measurements may not be suitable to localize subfailure damage or appropriate as tolerance criteria for structural injury in this ligament.

Damage to the collagen extracellular matrix and the ensuing effects of such damage on the mechanical and cellular responses of that tissue have been reported for subfailure loading of ligaments and tendons. Provenzano et al. reported that nonrecoverable laxity in rat medial collateral ligaments was initiated at slightly less than half the strain required to produce tissue failure and that this type of loading also corresponded to a decrease in cell viability (35) and an initiation of fibroblast-mediated remodeling (34). Laxity has also been noted in other soft tissues as a result of some subfailure loading conditions (20, 30, 33), and changes in ligament stiffness or tangential modulus have also been reported (29, 30, 35). The detection of damage via changes in collagen fiber rotation at 51 ± 12% of the displacement for gross failure (Table 1) in our study further supports the hypothesis that collagen fiber damage may produce nonrecoverable laxity, joint instability, and the initiation of collagen matrix remodeling. Although mechanistic studies are required to understand the putative nociceptive and inflammatory responses leading to pain that follow the initiation of tissue damage in the facet capsule, the relative percentage (12.65 ± 6.69%) of the failure energy required for damage in the present study is sufficient to also produce yield and sustained modifications in the collagen fiber alignment of the rat facet capsule, as well as persistent symptoms in an in vivo painful facet capsular ligament model in the rat (36, 37). Together, those reports and our present findings imply that the increases in the rotation of collagen fibers observed during loading in the present study may be sufficient to produce nonrecoverable damage. Future work is required to directly determine whether this damage is capable of inciting sustained physiological consequences such as persistent pain. The present study provides a novel method to determine the loading conditions, location, and potentially fiber-based mechanisms that can produce collagen fiber injury, which ultimately may enable a more refined interpretation of the ensuing physiological consequences associated with structural damage in ligaments.

The present fiber kinematic data suggest a number of potential mechanisms that can lead to structural damage, ligament yield, and, ultimately, potential permanent physiological dysfunction. The significant correlation between yield and evidence of altered fiber kinematics during initial damage suggests that these two metrics may be different measurements of the same injury and evidence of microstructural damage manifesting itself in the macroscale stiffness response observed as yield. Since altered fiber kinematics were initially identified before yield in three specimens (Table 1), our fiber rotation-based damage metric may be more sensitive for detecting

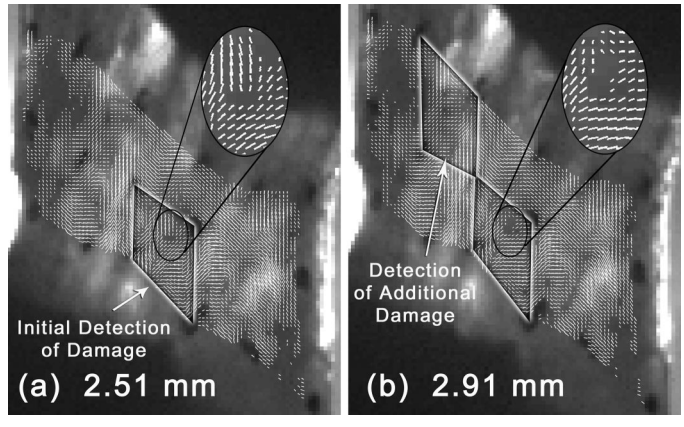

Fig. 4. Fiber alignment maps of *specimen C390-C45L* during and after initial detection of damage. Collagen fiber alignment exhibited great spatial variability upon initial detection of damage (*a*). Arrow, damaged element. *Inset*: subregion where the majority of fiber realignment occurred (circled region). After an additional 0.4 mm of distraction (*b*), the element where damage was initially detected in (*a*) had undergone substantial realignment, which persisted until failure. *Inset*: magnification of the same subregion in *a.* Note shift in alignment of fibers toward the horizontal. At 2.91 mm, a second element was also detected as damaged (*top left* in *b*); yield was detected at 2.92 mm of distraction for this specimen (see Table 1).

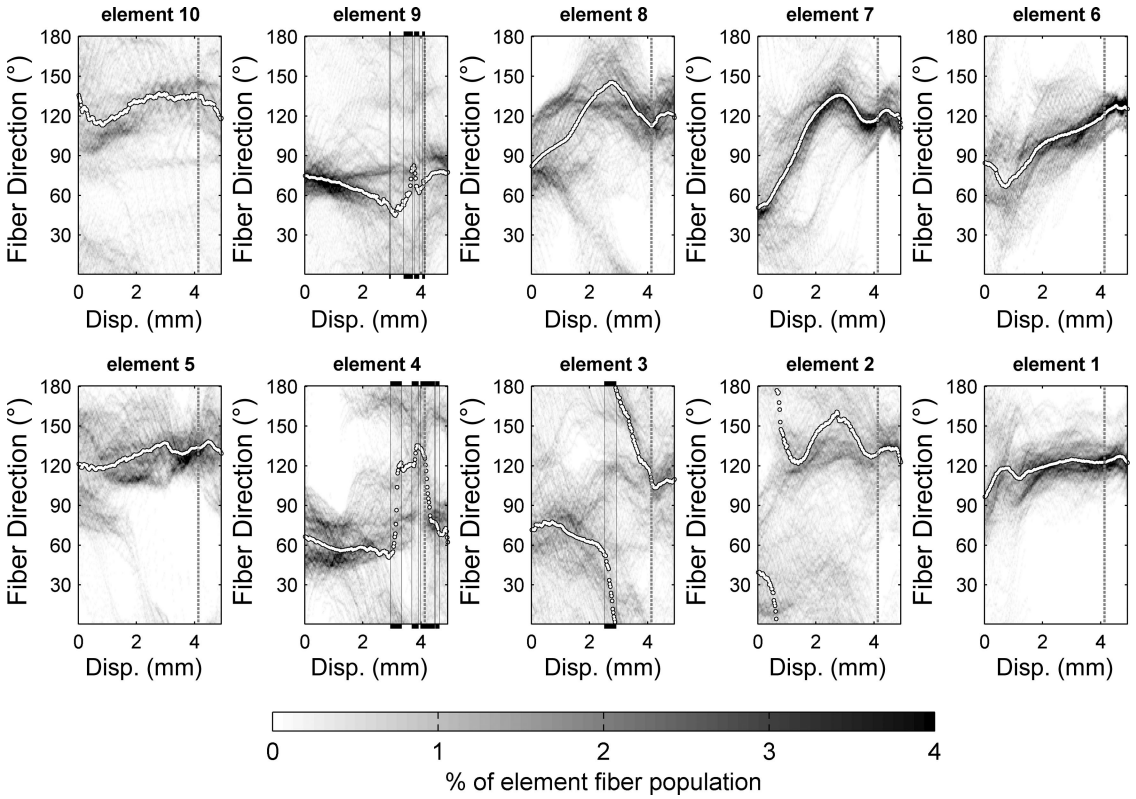

Fig. 5. Fiber alignment vs. displacement for each element in *specimen C390-C45L*. For some regions of the capsule, distribution of fiber directions changed substantially with increasing displacement. Damage was often detected (black horizontal bars on *x*-axis) when fiber alignment within an element became highly varied and mean fiber direction (white markers with black border) underwent significant rotation. First detection of damage for this specimen was in *element 3* at 2.51 mm. Although mean fiber direction initially fluctuated in *element 2* during the first 1 mm of distraction, element- and displacement-specific standard deviation measurements prevented damage detection in that element at the beginning of distraction. Dotted line at 4.13 mm in every element plot indicates tissue failure. For each element, fiber direction from every pixel was binned in 1° increments at every 20 μm of displacement and is expressed as percentage of total number of pixels.

damage than yield in loading conditions where continued fiber recruitment can offset the putative microfailures that have been hypothesized to produce the phenomenon of yield (43, 54). Previous reports demonstrating the realignment of collagen fibers in engineered constructs at the beginning of yielding (43) further support this assertion. The regional increases in the rotation of collagen fiber direction during the detection of damage found in the present study (Figs. 4 and 5) may be evidence of the formation of microtears in localized regions of the collagen matrix. Increases in tissue stiffness were also noted after the initial detection of damage and yield (Fig. 2), which suggests that such initial microtears could result from the breaking of fiber cross-links before the ultimate failure of the load-bearing collagen fibers. Although the mean fiber direction in some regions of our samples did not rotate toward the direction of loading, even after damage (Fig. 5), nonaffine fiber kinematics have also been demonstrated after loading to high strains in other planar soft tissues (2). Nonaffine fiber network models have previously been implemented to describe the mechanical response of collagen constructs (7, 41) and may help further define the complex relationship between fiber kinematics and tissue loading for this capsular ligament. The creation of such a microstructural model could also help explain the development of microstructural damage and the contributions of fiber-dependent regional variability in injury tolerance for this tissue. However, more uniformly aligned materials may not require such a nonaffine microstructural model, and additional experimental studies with other ligaments could help assess the accuracy of this methodology and its broader applicability to other tissues. The present data, nonetheless, demonstrate a complex fiber kinematic response to joint distraction that will be important in understanding how potentially injurious loading to the collagen network may impose abnormal forces on the fibroblasts and/or afferent pain fibers in this ligament.

The present study is the first, to our knowledge, to demonstrate the integrated acquisition of continuous fiber alignment information during loading across an entire ligament midsubstance. To rapidly acquire microstructural data spanning a surface with substantial cross-sectional area, we defined fiber alignment at individual pixels. As a result, the orientation and position of individual collagen fibers could not be imaged; instead, regions of the tissue were used for analysis. Accordingly, for the present study, damage and strain were localized to elements on the basis of an array of fiduciary markers (Fig. 1). An increase in the spatial density of those markers or advanced image registration techniques could help further evaluate and refine the accuracy and precision in defining the location of damage using this fiber rotation-based detection technique. Although the acquisition of fiber alignment data was limited to two dimensions in the present study, the retardation data suggest that the extent of fiber alignment through the

thickness of this tissue may not be different between damaged and undamaged regions of the tissue (Table 2). The incorporation of retardation data into the damage metric in the future may help refine its accuracy in detection, but it will be necessary to account for sample thickness variation because of its effect on the retardation measurements. Complementary electron microscopy studies capturing evidence of damage or modified organization in the capsular ligament microstructure after loading are needed to determine the severity and the underlying mechanisms of the microstructural failure that is detected by the regional change in fiber alignment here. Although the present study reports results from a small sample size, the damage detected at gross ligament failure propagated into obvious tissue tears in all four specimens that failed within the elements covering the midsubstance of the ligament (Fig. 3). Including the 88 total elements from all specimens, the high odds ratio for our fiber rotation-based metric to correctly identify the location of rupture within the analyzed element regions demonstrates a strong association between that metric and gross tissue damage and may actually underestimate that association, given that damage was detected in multiple regions at failure for some specimens (Fig. 3). The propagation of microtears into visible rupture is likely dependent on the severity of the initial damage and the alignment of the collagen matrix surrounding that damage. Given the spatial variability of the collagen alignment in this tissue (Fig. 4), the simultaneous development of visible ruptures from all regions detected as being damaged at failure would not be expected. By utilizing QPLI data in the development of a collagen rotation-based metric for damage, the present study helps lay a foundational framework to define mechanistic relationships between tissue microstructure, deformation, and structural damage and suggests that strain thresholds for injury may need to be modified to reflect regional dependence or functionalized to incorporate measures of the underlying microstructure.

Strain is a common metric used to localize injury and define tissue tolerances (1, 5, 9, 14, 24, 25, 31) and is often used as a criterion in finite-element (11, 12, 26) and computational (7, 22, 28, 47) models to predict injury. However, the use of strain for these purposes may not always be appropriate for biological tissues in which macroscale measurements do not translate to similar microscale strain values. For example, strain at the microscale level is highly variable and does not correspond to macroscale deformations in tendon, annulus fibrosis, and meniscus tissue (3, 4, 8, 39, 46). In fact, these differences in strain measurements across length scales of the same tissue have been specifically attributed to the collagen fiber kinematics and organization (4, 7, 39). The discrepancy between the locations of maximum principal strain (Fig. 1) and damage (Fig. 4) in the present study may be due to the macroscale strain measurements inadequately representing the more local strains of the failing microstructural constituents or the inherent composition and organization of the facet capsule tissue. The present work, together with reports in the literature (3, 28, 32, 36, 39, 46), suggests that attempts to define strain thresholds for structural damage or physiological responses in ligament and other soft tissues may be highly dependent on the resolution of the strain measurements and the appropriate incorporation of fiber-level data.

Certainly, techniques such as QPLI offer promise for specifically defining relevant subfailure tissue responses; however, they require very specific testing protocols and specimen preparation to enable light transmission. Unless techniques that utilize backscattering to determine fiber alignment are integrated with the fiber-based damage detection approach presented here, QPLI and other polarized light methods will have limited utility in certain applications where noninvasive strain measurements can enable detailed characterization of tissue responses. However, integrative experimental approaches and studies at the tissue level that implement coordinated structure-, strain-, and fiber-based metrics will lead to a complete and more detailed understanding of the physical relationship between all these outcomes. The apparent disconnect between strain fields and potential collagen matrix damage in the present study highlights the utility of these methods for use in directly defining the tolerance of collagenous soft tissues to structural damage and in establishing injury thresholds that may be more relevant to pathophysiological outcomes.

GRANTS

This work was funded by grants from the Southern Consortium for Injury Biomechanics/National Highway Traffic Safety Administration, the Catharine D. Sharpe Foundation, and the Association for the Advancement of Automotive Medicine. This material is based on work supported by the National Science Foundation under Grant 0547451.

REFERENCES

1. **Bain AC, Meaney DF.** Tissue-level thresholds for axonal damage in an experimental model of central nervous system white matter injury. *J Biomech Eng* 122: 615–622, 2000.
2. **Billiar KL, Sacks MS.** A method to quantify the fiber kinematics of planar tissues under biaxial stretch. *J Biomech* 30: 753–756, 1997.
3. **Bruehlmann SB, Hulme PA, Duncan NA.** In situ intercellular mechanics of the bovine outer annulus fibrosus subjected to biaxial strains. *J Biomech* 37: 223–231, 2004.
4. **Bruehlmann SB, Matyas JR, Duncan NA.** Collagen fibril sliding governs cell mechanics in the anulus fibrosus—an in situ confocal microscopy study of bovine discs. *Spine* 29: 2612–2620, 2004.
5. **Cater HL, Sundstrom LE, Morrison B.** Temporal development of hippocampal cell death is dependent on tissue strain but not strain rate. *J Biomech* 39: 2810–2818, 2006.
6. **Cavanaugh JM, Ozaktay AC, Yamashita HT, King AI.** Lumbar facet pain: biomechanics, neuroanatomy and neurophysiology. *J Biomech* 29: 1117–1129, 1996.
7. **Chandran PL, Barocas VH.** Affine versus non-affine fibril kinematics in collagen networks: theoretical studies of network behavior. *J Biomech Eng* 128: 259–270, 2006.
8. **DeFrate LE, van der Ven A, Boyer PJ, Gill TJ, Li GA.** The measurement of the variation in the surface strains of Achilles tendon grafts using imaging techniques. *J Biomech* 39: 399–405, 2006.
9. **Deng B, Begeman PC, Yang KH, Tashman S, King AI.** Kinematics of human cadaver cervical spine during low speed rear-end impacts. *Stapp Car Crash J* 44: 171–188, 2000.
10. **Dickey JP, Hewlett BR, Dumas GA, Bednar DA.** Measuring collagen fiber orientation: a two-dimensional quantitative macroscopic technique. *J Biomech Eng* 120: 537–540, 1998.
11. **Einstein DR, Reinhall P, Nicosia M, Cochran RP, Kunzelman K.** Dynamic finite element implementation of nonlinear, anisotropic hyperelastic biological membranes. *Comput Methods Biomech Biomed Eng* 6: 33–44, 2003.
12. **Gardiner JC, Weiss JA.** Subject-specific finite element analysis of the human medial collateral ligament during valgus knee loading. *J Orthop Res* 21: 1098–1106, 2003.
13. **Geday MA, Kaminsky W, Lewis JG, Glazer AM.** Images of absolute retardance L. Deltan, using the rotating polariser method. *J Microsc* 198: 1–9, 2000.
14. **Gefen A, van Nierop B, Bader DL, Oomens CW.** Strain-time cell-death threshold for skeletal muscle in a tissue-engineered model system for deep tissue injury. *J Biomech* 41: 2003–2012, 2008.
15. **Gimbel JA, Van Kleunen JP, Mehta S, Perry SM, Williams GR, Soslowsky LJ.** Supraspinatus tendon organizational and mechanical prop-

erties in a chronic rotator cuff tear animal model. *J Biomech* 37: 739–749, 2004.
16. **Glazer AM, Lewis JG, Kaminsky W.** An automatic optical imaging system for birefringent media. *Proc R Soc Lond A* 452: 2751–2765, 1996.
17. **Hadian M, Corcoran BM, Han RI, Grossmann JG, Bradshaw JP.** Collagen organization in canine myxomatous mitral valve disease: an x-ray diffraction study. *Biophys J* 93: 2472–2476, 2007.
18. **Hansen KA, Weiss JA, Barton JK.** Recruitment of tendon crimp with applied tensile strain. *J Biomech Eng* 124: 72–77, 2002.
19. **Hurschler C, Provenzano PP, Vanderby R.** Scanning electron microscopic characterization of healing and normal rat ligament microstructure under slack and loaded conditions. *Connect Tissue Res* 44: 59–68, 2003.
20. **Iatridis JC, MacLean JJ, Ryan DA.** Mechanical damage to the intervertebral disc annulus fibrosus subjected to tensile loading. *J Biomech* 38: 557–565, 2005.
21. **Kliewer MA, Gray L, Paver J, Richardson WD, Vogler JB, McElhaney JH, Myers BS.** Acute spinal ligament disruption—MR imaging with anatomic correlation. *J Magn Reson Imaging* 3: 855–861, 1993.
22. **Lanir Y.** Constitutive equations for fibrous connective tissues. *J Biomech* 16: 1–12, 1983.
23. **Lee KE, Franklin AN, Davis MB, Winkelstein BA.** Tensile cervical facet capsule ligament mechanics: failure and subfailure responses in the rat. *J Biomech* 39: 1256–1264, 2006.
24. **Lee KE, Thinnes JH, Gokhin DS, Winkelstein BA.** A novel rodent neck pain model of facet-mediated behavioral hypersensitivity: implications for persistent pain and whiplash injury. *J Neurosci Methods* 137: 151–159, 2004.
25. **Lu Y, Chen C, Kallakuri S, Patwardhan A, Cavanaugh JM.** Neurophysiological and biomechanical characterization of goat cervical facet joint capsules. *J Orthop Res* 23: 779–787, 2005.
26. **Mao H, Zhang L, Yang KH, King AI.** Application of a finite element model of the brain to study traumatic brain injury mechanisms in the rat. *Stapp Car Crash J* 50: 583–600, 2006.
27. **Matcher SJ, Winlove CP, Gangnus SV.** The collagen structure of bovine intervertebral disc studied using polarization-sensitive optical coherence tomography. *Phys Med Biol* 49: 1295–1306, 2004.
28. **Meaney DF.** Relationship between structural modeling and hyperelastic material behavior: application to CNS white matter. *Biomech Model Mechanobiol* 1: 279–293, 2003.
29. **Panjabi MM, Moy P, Oxland TR, Cholewicki J.** Subfailure injury affects the relaxation behavior of rabbit ACL. *Clin Biomech* 14: 24–31, 1999.
30. **Panjabi MM, Yoldas E, Oxland TR, Crisco JJ 3rd.** Subfailure injury of the rabbit anterior cruciate ligament. *J Orthop Res* 14: 216–222, 1996.
31. **Pearson AM, Ivancic PC, Ito S, Panjabi MM.** Facet joint kinematics and injury mechanisms during simulated whiplash. *Spine* 29: 390–397, 2004.
32. **Phatak NS, Sun Q, Kim SE, Parker DL, Sanders RK, Veress AI, Ellis BJ, Weiss JA.** Noninvasive determination of ligament strain with deformable image registration. *Ann Biomed Eng* 35: 1175–1187, 2007.
33. **Pollock RG, Wang VM, Bucchieri JS, Cohen NP, Huang CY, Pawluk RJ, Flatow EL, Bigliani LU, Mow VC.** Effects of repetitive subfailure strains on the mechanical behavior of the inferior glenohumeral ligament. *J Shoulder Elbow Surg* 9: 427–435, 2000.
34. **Provenzano PP, Alejandro-Osorio AL, Valhmu WB, Jensen KT, Vanderby R Jr.** Intrinsic fibroblast-mediated remodeling of damaged collagenous matrices in vivo. *Matrix Biol* 23: 543–555, 2005.
35. **Provenzano PP, Heisey D, Hayashi K, Lakes R, Vanderby R Jr.** Subfailure damage in ligament: a structural and cellular evaluation. *J Appl Physiol* 92: 362–371, 2002.
36. **Quinn KP, Lee KE, Ahaghotu CC, Winkelstein BA.** Structural changes in the cervical facet capsular ligament: potential contributions to pain following subfailure loading. *Stapp Car Crash J* 51: 169–187, 2007.
37. **Quinn KP, Winkelstein BA.** Cervical facet capsular ligament yield defines the threshold for injury and persistent joint-mediated neck pain. *J Biomech* 40: 2299–2306, 2007.
38. **Sasaki N, Shukunami N, Matsushima N, Izumi Y.** Time-resolved X-ray diffraction from tendon collagen during creep using synchrotron radiation. *J Biomech* 32: 285–292, 1999.
39. **Screen HRC, Lee DA, Bader DL, Shelton JC.** An investigation into the effects of the hierarchical structure of tendon fascicles on micromechanical properties. *Proc Inst Mech Eng Pt H–J Eng Med* 218: 109–119, 2004.
40. **Siegmund GP, Myers BS, Davis MB, Bohnet HF, Winkelstein BA.** Mechanical evidence of cervical facet capsule injury during whiplash: a cadaveric study using combined shear, compression, and extension loading. *Spine* 26: 2095–2101, 2001.
41. **Thomopoulos S, Fomovsky GM, Chandran PL, Holmes JW.** Collagen fiber alignment does not explain mechanical anisotropy in fibroblast populated collagen gels. *J Biomech Eng* 129: 642–650, 2007.
42. **Thomopoulos S, Williams GR, Gimbel JA, Favata M, Soslowsky LJ.** Variation of biomechanical, structural, and compositional properties along the tendon to bone insertion site. *J Orthop Res* 21: 413–419, 2003.
43. **Tower TT, Neidert MR, Tranquillo RT.** Fiber alignment imaging during mechanical testing of soft tissues. *Ann Biomed Eng* 30: 1221–1233, 2002.
44. **Tower TT, Tranquillo RT.** Alignment maps of tissues. I. Microscopic elliptical polarimetry. *Biophys J* 81: 2954–2963, 2001.
45. **Tower TT, Tranquillo RT.** Alignment maps of tissues. II. Fast harmonic analysis for imaging. *Biophys J* 81: 2964–2971, 2001.
46. **Upton ML, Gilchrist CL, Guilak F, Setton LA.** Transfer of macro-scale tissue strain to micro-scale cell regions in the deformed meniscus. *Biophys J* 94: 2116–2124, 2008.
47. **Vande Geest JP, Sacks MS, Vorp DA.** A planar biaxial constitutive relation for the luminal layer of intra-luminal thrombus in abdominal aortic aneurysms. *J Biomech* 39: 2347–2354, 2006.
48. **Wedeen VJ, Reese TG, Napadow VJ, Gilbert RJ.** Demonstration of primary and secondary muscle fiber architecture of the bovine tongue by diffusion tensor magnetic resonance imaging. *Biophys J* 80: 1024–1028, 2001.
49. **Whittaker P, Canham PB.** Demonstration of quantitative fabric analysis of tendon collagen using two-dimensional polarized light microscopy. *Matrix* 11: 56–62, 1991.
50. **Williams RM, Zipfel WR, Webb WW.** Interpreting second-harmonic generation images of collagen I fibrils. *Biophys J* 88: 1377–1386, 2005.
51. **Winkelstein BA, Nightingale RW, Richardson WJ, Myers BS.** The cervical facet capsule and its role in whiplash injury: a biomechanical investigation. *Spine* 25: 1238–1246, 2000.
52. **Yahia L, Brunet J, Labelle S, Rivard CH.** A scanning electron microscopic study of rabbit ligaments under strain. *Matrix* 10: 58–64, 1990.
53. **Yang KH, King AI.** Neck kinematics in rear-end impacts. *Pain Res Manag* 8: 79–85, 2003.
54. **Yoganandan N, Ray G, Pintar FA, Myklebust JB, Sances A.** Stiffness and strain energy criteria to evaluate the threshold of injury to an intervertebral joint. *J Biomech* 22: 135–142, 1989.